



Atmosphere Influence on Oxidation at High Temperature of Ni–Cr–Si Model Alloys

Marion Poncet¹ · Christophe Issartel¹ · Sébastien Perrier¹ · Henri Buscail¹

Received: 4 June 2021 / Revised: 4 June 2021 / Accepted: 8 June 2021 /
Published online: 14 July 2021

© The Author(s), under exclusive licence to Springer Science+Business Media, LLC, part of Springer Nature 2021

Abstract

The use of nitriding and carburizing atmospheres in industrial furnaces leads to a drastic reduction in their lifetime. In order to enhance protection, a pre-oxidation step of the chromia-forming alloys used in the furnaces is necessary. The aim of this study is to show the influence of the gaseous environment on the degradation resistance of a pre-oxidized Ni–Cr–Si model alloy at 950 °C. Two different gaseous environments were used: dry air and nitrogen containing 5 volume % of hydrogen (N₂–5%H₂). After dry air oxidation, a continuous amorphous SiO₂ subscale was formed at the chromia/metal interface. After oxidation in N₂–5%H₂, containing 20 ppmv oxygen, a non-continuous crystalline SiO₂ subscale is observed.

Keywords Chromia · High temperature oxidation · N₂–5vol.%H₂ · Silica · Nickel model alloys · Cristobalite

✉ Marion Poncet
marion.poncet@uca.fr

Christophe Issartel
christophe.issartel@uca.fr

Sébastien Perrier
sebastien.perrier@uca.fr

Henri Buscail
henri.buscail@uca.fr

¹ LVEEM, Université Clermont Auvergne, 8 Rue Jean Baptiste Fabre, 43000 Le Puy en Velay, France

Introduction

Many alloys are used in furnaces for high-temperature carburizing and nitriding treatments. These deleterious environments induce serious degradations of the alloys and lead to a significant reduction in the furnace's lifespan [1]. To improve the carburizing resistance, high nickel containing alloys are considered.

These alloys are known to decrease the thermodynamic stability of chromium carbide and the carbon permeability [2]. As proposed in the literature, the presence of an adherent oxide layer as a diffusion barrier is expected [1, 3–6]. Thus, on chromia forming alloys, the oxidation under isothermal conditions leads to a protective layer [5, 7–9]. However, other studies [10] show that a high chromium content is required to decrease the oxidation rate and carburization in pure CO₂. Moreover, silicon addition can be beneficial against carburization by forming a protective silica layer at the metal/oxide interface [4, 6, 8, 9, 11–16]. Usually, the silicon is not added at more than 1 weight % in the alloy. In our study, the Ni–Cr–Si alloy contains 2 weight % silicon. This silicon content is sufficient to obtain a silica sublayer [17–20] and the formation of a Cr₃Si intermetallic in the alloy[21].

The gaseous environment is one important factors influencing the oxide layer formation [22]. Previous studies have shown that oxidation in air on ferritic chromia forming alloys containing 2 weight % silicon leads to a bad adherent chromia scale [23] and a non-continuous silica sublayer [17–20]. However, on a ferritic steel, a protective and continuous silica sublayer is favored by a low oxygen containing gaseous environment and a high silicon content [12, 24].

The influence of the atmosphere on the high temperature oxidation of nickel–chromium–silicon model alloys will be investigated in this paper. Two atmospheres with various oxygen partial pressure ($p(\text{O}_2)$) are considered: ambient air with 20.9 vol.% O₂ [25] and N₂–5%H₂ containing 20 ppmv O₂. The N₂–5%H₂ gaseous environment corresponds to industrial heat treatment conditions with low oxygen and high nitrogen potentials. Dorcheh et al. [26] have shown the formation of stable nitride Cr₂N and CrN on a chromium alloy oxidized at 950 °C in this gaseous condition. Then, oxidation and nitridation resistances are improved by a high silicon and chromium content for iron–chromium–silicon model alloys [27]. Moreover, Issartel et al.[12] have shown that silica crystallization is favored at the metal/oxide interface. Thus, under low oxygen conditions, a silica sublayer associated with an adherent chromia scale can be a good protective barrier against carburization. The aim of the present work is to determine if it is possible to build the same type of protective oxide barrier on a model nickel–chromium–silicon alloy.

The influence of a gaseous environment on the oxidation kinetics of Ni–Cr–Si model alloys at 950 °C has been followed by thermogravimetric analysis (TGA). The phase identification has been carried out by X-ray diffraction (XRD) and scanning electron microscopy (SEM).

Experimental Procedures

Sample Preparation

A Ni–Cr–Si model alloy was manufactured by the team “Surface and Interface, Chemical Reactivity of Materials <https://ijl.univ-lorraine.fr/en/research/departements-scientifiques/chemistryand-physics-of-solids-and-surfaces-department/surface-and-interface-chemical-reactivity-of-materials/>” (SIRCM) at the “Jean Lamour” Institute in Nancy (France). The alloys have been prepared by high frequency melting leading to the following composition (Table 1).

Chemical elements of purity greater than 99.95% were placed in a water-cooled copper crucible and enclosed in a silica tube. Before each mixing, three to four argon aspiration and filling sequences were carried out to clean the reactor gaseous environment. To avoid important volatilization of the metallic elements, melting was carried out in argon at a pressure of 0.8 atm. The metallic mixture obtained was then melted three times to ensure a homogeneous distribution of the elements. Then, the ingot was gravity cast in a cold copper mold to obtain cylinders of 10 mm in diameter. Cylindrical samples with a surface area of approximately 1.8 cm² were then cut from the metal bar. Finally, the samples were mechanically abraded up to the 1200 grade SiC paper, then degreased with acetone and dried.

Oxidation Process and Analyses

The rate of oxidation at high temperature was followed by thermogravimetric analysis (TGA) in isothermal conditions using a Setaram TG - DTA 92–1600 micro-thermobalance. These analyses were conducted at 950 °C for 70 h with an 8 l/h flow rate either in air (1 atm.) or in nitrogen containing 5 vol. % hydrogen (N₂–5%H₂). An Elcowa GPR1200MS oxygen analyzer was used to measure the 20 ppmv residual O₂ content.

To test the reproducibility, three samples were oxidized using the same conditions. The oxide identification was carried out by X-ray diffraction (XRD) using a Philips X’pert diffractometer with K α =0,15,406 nm copper radiation. The XRD patterns were recorded for 8 h using a 0,02° step, 2 θ ranges from 18° to 68° and the counting time is 12 s. For reproducibility, all analyses have been performed twice.

The surface and cross-sectional oxide morphologies were observed by use of a JEOL 7600 scanning electron microscope coupled to a LINK energy-dispersive X-ray spectroscope EDXS (ICB, Dijon “<https://icb.u-bourgogne.fr/procedesmetallurgiques-durabilite-materiaux-pmdm/>”). The EDXS point analyses were performed with an electron probe focused on a spot of 1 μ m diameter.

Table 1 Alloy composition in wt.% and at.% of the Ni–Cr–Si samples used in the study

	Ni	Cr	Si
Composition (wt.%)	72.5	25.5	2.0
Composition (at.%)	75.5	23.5	1.0

Results

Oxidation Kinetics

The TGA was performed in a controlled atmosphere and the measured mass change per unit area $\Delta m/S$ is plotted on Fig. 1 after oxidation in air and $N_2-5\%H_2$.

Kinetics curves follow a parabolic law. It indicates that oxide growth is controlled by diffusion of ionic species through the thickening oxide scale [28]. For oxidized chromia-forming alloys above 950 °C, the oxidation kinetics can deviate from the ideal diffusion limited behavior due to volatilization and the formation of defects (spallation and, cracking, etc.). This implies a multi-step oxidation process [29]. It is therefore necessary to determine the parabolic rate constant k_p , and the volatilization rate constant k_v (Eq. 1):

$$\Delta m/S = \sqrt{k_p t} - k_v t \quad (1)$$

where Δm is the mass change, S is the surface area and t is time. The calculation of the parabolic rate constants is extracted from the slope of $\Delta m/S = f(\sqrt{t})$ (Fig. 2), [30]. The results are presented in Table 2.

Firstly, for each atmosphere studied, the mass gain is the same after 70 h oxidation (Fig. 1).

In air, Fig. 2 shows that before 25 h ($\sqrt{t}=300 \text{ s}^{1/2}$), the mass gain follows a parabolic law. This indicates a regime governed by ion diffusion through the oxide layer [28]. After 25 h, the oxidation rate decreases. This reveals a competition between the mass gain of the diffusion regime and the mass loss due to the chromia volatilization of chromia at 950 °C. The volatilization rate constant k_v is therefore calculated according to Eq. 1.

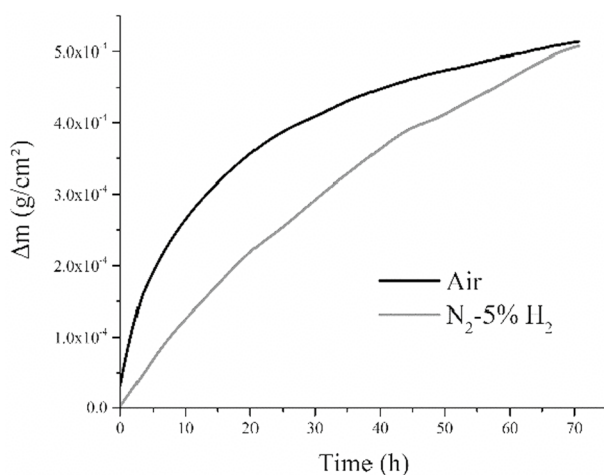


Fig. 1 Mass gain curves versus time for the Ni–Cr–Si alloy oxidized at 950 °C, 70 h, in air (black) and in $N_2-5 \text{ vol\% } H_2$ (grey)

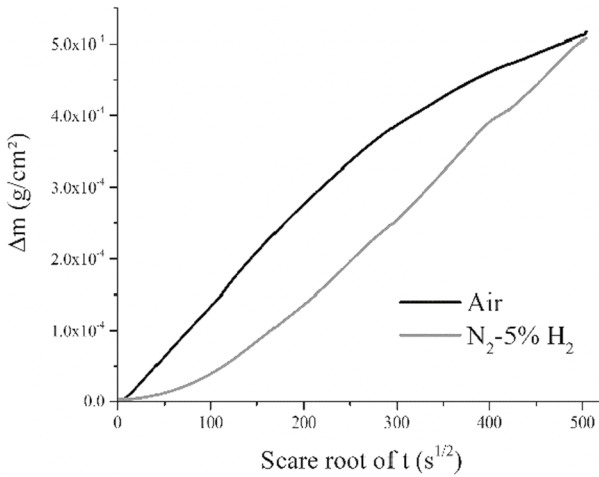


Fig. 2 Mass gain versus \sqrt{t} plot after oxidation in air (black) and N_2 -5% H_2 (gray)

Table 2 Results of parabolic and volatilization velocity constants computation under air and N_2 -5% H_2

Atmosphere	k_p ($g^2 \cdot cm^{-4} \cdot s^{-1}$)	k_v ($g \cdot cm^{-2} \cdot s^{-1}$)
Air	2.7×10^{-12}	1.2×10^{-9}
N_2 -5% H_2	1.5×10^{-12}	0

After N_2 -5% H_2 oxidation, the kinetic curve initially follows a linear law characteristic of the germination of an oxide layer on a metallic surface. This first step is longer under N_2 -5% H_2 because the oxygen available in the gaseous environment is lower than in air. After 2 h and 40 min ($\sqrt{t}=100 \text{ s}^{1/2}$), the curve follows a parabolic law indicating that the limiting factor is a diffusional process through the oxide layer. It comes from the assumption that no volatilization occurs at such low oxygen partial pressure, which is consistent with the TGA recorded after 70 h.

According to the fitting equation of the air oxidation curve, k_p et k_v are calculated (Table 2).

The values of k_v satisfy Dorcheh et Galetz condition [29] which postulates that k_v is at least two orders of magnitude greater than k_p . G.A. Green et al. [31] show the evolution of k_p as a function of temperature for an Inconel 718 (52.2wt.%Ni, 19wt.%Cr and 21wt.%Fe) and their estimation leads to a k_p at $1.7 \times 10^{-11} \text{ g}^2 \text{ cm}^{-4} \text{ s}^{-1}$. Our results show that values obtained are one order of magnitude lower. It is related to the fact that our samples are iron free.

Present results also indicate that the parabolic rate constant is twice higher for oxidation under air than under N_2 -5% H_2 . Moreover, the volatilization of chromia occurs only at high partial pressure in O_2 (in air). The k_v order of magnitude is about 3 times greater than for k_p showing its importance on the oxidation kinetic. It justifies that, the mass gain of the samples after 70 h of oxidation is identical in both gas despite a higher parabolic rate constant in air.

XRD Analysis

X-ray diffraction permits the crystalline phases identification on the specimen's surface after oxidation. XRD patterns are presented on Fig. 3.

In each gaseous environment, the FeNi_3 substrate (ICDD 38–0419) is well detected indicating that the oxide layer is relatively thin. The FeNi_3 peaks intensity is more pronounced after oxidation in N_2 –5% H_2 than in air. This indicates that the chromia (ICDD 38–1479) scale is thinner. In N_2 –5% H_2 , the XRD pattern shows that SiO_2 cristobalite (ICDD 39–1425) is also present on the surface.

Scale Morphology

SEM surface (Fig. 4) and cross section (Fig. 5) morphologies are presented as follows.

After oxidation in both gaseous environments, two main gray scale aspects can be distinguished on the BSE images: a light gray surface morphology identified as chromia and darker areas corresponding to the silica sublayer.

In air (Fig. 4a), the lighter areas correspond to the metallic surface. It corresponds to spalled areas. It also appears that the chromia scale is more adherent on the silica sublayer than to the alloy itself. Chromia grains show a faceted structure as it was observed by Issartel et al. [12] on model Fe–Cr–Si samples.

The oxidation in N_2 –5% H_2 does not show any spalled areas (Fig. 4b). However, the chromia layer is not completely covering the alloy surface. In between, SEM imaging reveals that the SiO_2 subscale can be directly in contact with the gaseous environment. Chromia grains have not the same structure compared to air oxidation. They show a spherical and porous structure as observed by Issartel et al. [12] on a ferritic alloy.

Cross-sectional morphologies are presented on Fig. 5 and Fig. 6. The silica subscale is thicker after oxidation in N_2 –5% H_2 (1.5 μm) than in air (0.3 μm). The

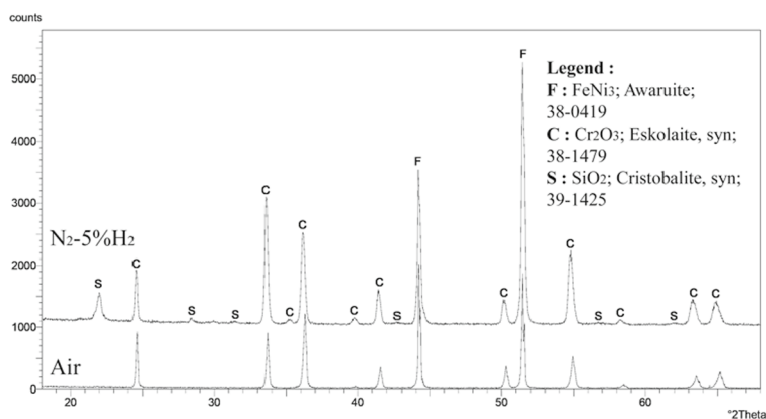


Fig. 3 XRD patterns obtained on Ni–Cr–Si oxidized at 950 °C during 70 h in air and N_2 –5% H_2

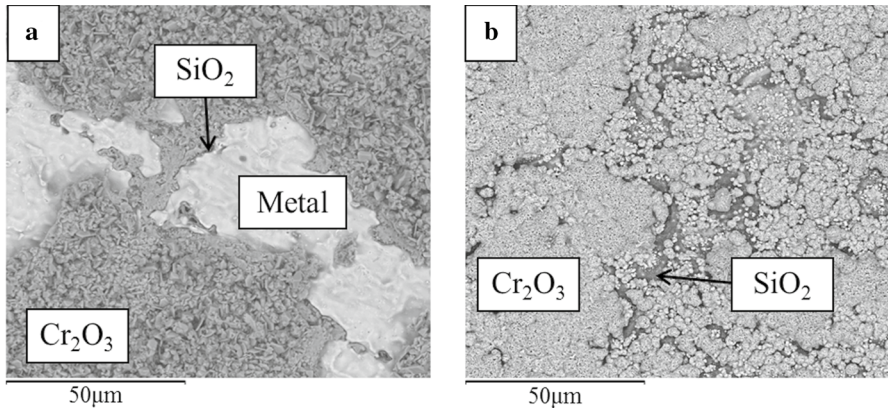


Fig. 4 BSE images of Ni–Cr–Si samples surfaces oxidized at 950 °C, **a** in air and **b** N_2 -5% H_2

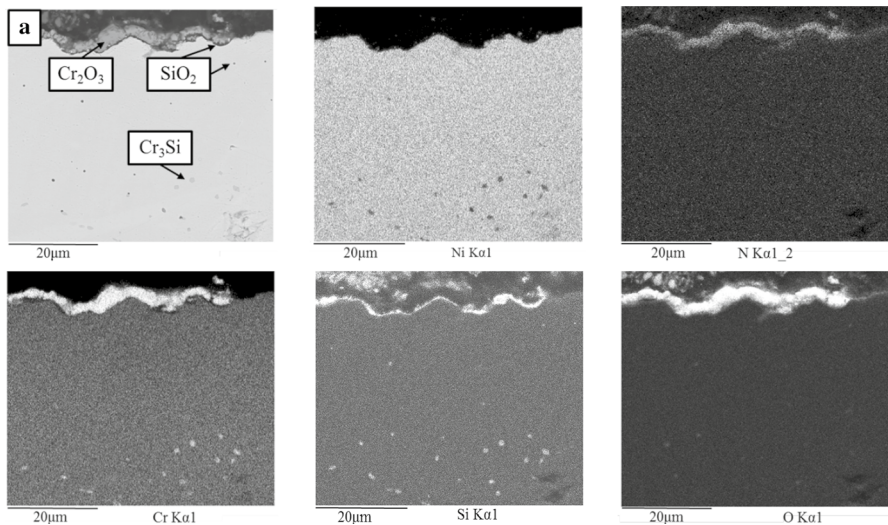


Fig. 5 Cross-sectional BSE image **a** and X-mapping pictures for Ni–Cr–Si samples oxidized in air

thickness of the chromia layer is between 2.4 and 2.7 μm . These values are not significant because polishing has removed a part of them. SiO_2 at the internal interface and Cr_3Si precipitates in the metallic matrix are observed due to the high silicon alloy content [21].

After air oxidation (Fig. 5), oxide spallation and a wavy silica/metal interface are observed. This wavy interface could promote scale spallation. The silica subscale is continuous at the metal/chromia interface. Cr_3Si phase depletion is observed 30 μm thick inside the metal under the scale.

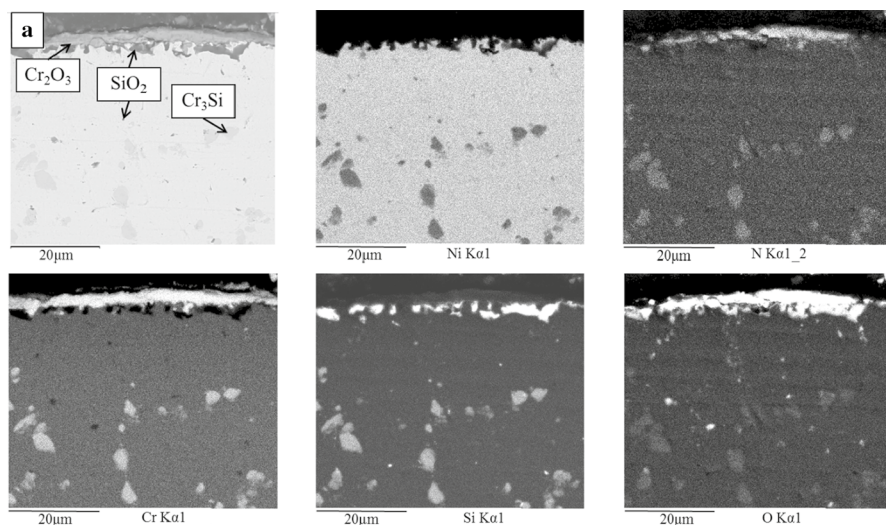


Fig. 6 Cross-sectional BSE image **a** and X-mapping pictures for Ni–Cr–Si samples oxidized in N_2 –5% H_2

Finally, X-mapping of nitrogen revealed the presence of nitrogen in the chromia layer. However, no trace of nitrogen is found in the silica sublayer.

After N_2 –5% H_2 oxidation (Fig. 6), the silica nodules are large and located inside the matrix. Cr_3Si nodule depletion is observed 20 μm deep inside the metal. These intermetallic zones are more numerous, their size is larger. EDXS point analysis on the chromia layer and Cr_3Si intermetallic nodules indicate that nitrogen is more present than after air oxidation.

Discussion

In order to improve oxidation and nitridation resistance, the use of silicon has already proven its efficiency [12] on an iron-chromium-silicon model alloy (Fe–Cr–Si). It has been shown in previous works [4, 6, 8, 9, 11–16, 32, 33] that a protective silica sublayer is present at the alloy/chromia scale interface [12].

In the present work, the silica subscale formation is also observed on oxidized Ni–Cr–Si specimens. Moreover, a crystalline form of silica has also been observed (cristobalite).

Oxidation in air

The air oxidation kinetics of a Ni–Cr–Si alloy follows a parabolic law indicating a diffusional regime limited by Cr^{3+} ions through the chromia rhombohedral lattice (ICDD 38–1479) [34].

As mentioned by Stearns et al. [35] chromia volatilization is only observed at the high oxygen partial pressure present in air. With time, this phenomenon leads to the chromia layer weakening and does not allow to improve the oxidation resistance in a durable way.

According to Hussey [36], the transport mechanism in chromia is predominantly due to Cr^{3+} diffusion. This growth process induces coalescence of cationic vacancies at the metal/oxide interface and promotes void formation. Scale spallation effectively occurred after cooling to room temperature as observed on Fig. 4a. A continuous, thin and amorphous silica layer is located between chromia and the alloy and can also promote scale spallation [37].

Precipitates of intermetallic phases Cr_3Si were also observed in the matrix due to the high level of silicon in the alloy [21]. However, cross-sectional observations indicate that there is a Cr_3Si depletion 30 μm deep inside the alloy. Johnston [38] has examined the diffusion mechanism in Ni–Cr–Si alloys and found that increasing the silicon content increased chromium diffusion by about 20%. In the present work, it appears that chromium released from Cr_3Si permit chromia scale formation and free silicon could diffuse to build a protective silica scale (Fig. 5). Silica is amorphous in this case as shown on the XRD pattern (Fig. 3).

To conclude, observations made on the Ni–Cr–Si model alloy oxidized in air, at 950 °C are consistent with former studies. A non-adherent chromia scale formed along with an amorphous silica scale at the chromia/alloy interface.

Oxidation in N_2 –5% H_2

There are not so many studies about oxidation in N_2 –5 vol% H_2 . In this gaseous mixture, oxidation is related to the presence of the measured 20 ppmv O_2 content. SEM-EDXS results show the presence of a silica subscale between the alloy and chromia scale (Fig. 6). Intermetallic Cr_3Si nodules were also observed in the matrix due to the high level of silicon in the alloy [21]. After oxidation, the Cr_3Si depleted zone is 20 μm deep inside the alloy.

The main differences observed with air oxidation are shown by XRD and SEM analysis. After N_2 –5 vol% H_2 oxidation, a crystalline form of silica (cristobalite) is identified (Fig. 3) and no chromia scale spallation is observed (Fig. 4b).

The oxidation kinetics of a Ni–Cr–Si alloy in N_2 –5% H_2 follows a parabolic law indicating a purely diffusive mode. Li [33] proposed that the formation of a SiO_2 layer between the Ni–Cr–Si alloy and its chromia scale leads to chromium diffusion being at least controlled by an amorphous silica layer, rather than alloy diffusion. In our case, silica is not amorphous but atomic radius of Cr^{3+} ions [39]

is sufficiently low to allow diffusion through the tetragonal cristobalite lattice defects [4]. Moreover, the calculated parabolic rate constants k_p indicate a faster diffusion process in air than in N_2 -5% H_2 . A thicker, non-continuous cristobalite subscale can be considered as a better diffusion barrier than a thin continuous amorphous SiO_2 subscale.

In N_2 -5% H_2 , the thin chromia layer shows similar porosities to what was observed by Issartel et al. [12] after Fe–Cr–Si oxidation. In this case, no scale spallation is observed. Onishi [40] has demonstrated that under low oxygen potential a very thin SiO_2 layer forms on a Fe–Si alloy because the diffusion rate of silicon is relatively high compared to the diffusion rate of oxygen. It is then concluded that internal oxidation of the silica layer occurs in a restricted oxygen partial pressure range. Then silica obtained in N_2 -5% H_2 atmosphere is more adherent than amorphous silica obtained in air. Chromia scale is also more adherent when internal oxidation occurs.

No nitrides have been detected in the scale by XRD. However due to the high N_2 partial pressure, it is proposed that the amount of interstitial nitrogen in chromia and Cr_3Si can be higher than the one observed after air oxidation. The Cr_3Si intermetallic nodules are also more numerous compared to air oxidation. This difference seems to be due to the higher nitrogen presence in the gas. However, the EDX analysis does not detect any trace of nitrogen in the silica sublayer. Nevertheless, nitrogen is more present in the Cr_3Si intermetallic. This indicates that the silica sublayer does not inhibit nitrogen diffusion and does not play an effective barrier against nitriding.

Recently, Slimani [41] observed cristobalite formation after 1000 h oxidation of a Cr–Si alloy at 1200 °C, in air. In the present work a cristobalite structure was observed at relatively low temperature (950 °C), in air. It seems that the N_2 -5% H_2 gas mixture plays an important role in the silica crystallization. It is proposed that, nitrides, in undetectable amount by the techniques used, could act as nucleation site for silica crystallization.

Conclusion

The low oxygen containing N_2 -5% H_2 gaseous environment, was used to simulate industrial heat treatment conditions. This study has shown the influence of the oxygen partial pressure on Ni–Cr–Si oxidation for 70 h, at 950 °C. In both gaseous environments, a SiO_2 sublayer is formed. It indicates that this nickel-based alloy improves the silicon diffusion compared to an iron-base alloy with the same silicon content. After air oxidation, the silica sublayer formed is amorphous and chromia volatilization is observed.

After N_2 -5% H_2 oxidation, cristobalite is formed. A porous, and more adherent, chromia scale is also observed. No nitrides could be detected by XRD. However, EDXS has shown that nitrogen is present in the chromia layer and in the Cr_3Si intermetallic nodules. It is proposed that a very small nitride amount could promote silica crystallization.

Acknowledgements This work was supported in part by funding Laboratoire Vellave sur l'Elaboration et l'Etude des Matériaux.

References

1. French. Antoni, L. & Galerie, A. Techniques de l'Ingénieur, traité Matériaux métalliques Réf : m4224 29 (2002).
2. Olivares, R. I., Stein, W., Nguyen, T. D. & Young, D. J. Adv. Mater. Technol. Foss. Power Plants 889 (2016).
3. M. J. Bennett, J. A. Desport, and P. A. Labun, *Oxidation of Metals* **22**, 1984 (291–306).
4. R. C. Lobb, J. A. Sasse, and H. E. Evans, *Materials Science and Technology* **5**, 1989 (828–834).
5. A. Schnaas and H. J. Grabke, *Oxidation of Metals* **12**, 1978 (387–404).
6. G. Southwell, S. MacAlpine, and D. Young, *Journal of Materials and Science and Engineering* **88**, 1987 (81–87).
7. Jiang, C., Xie, Y., Kong, C., Zhang, J. & Young, D. J. *Corros. Sci.* **174**, 108801 (2020).
8. Nguyen, T. D., Zhang, J. & Young, D. J. **87**, 541 (2017).
9. R. I. Olivares, D. J. Young, T. D. Nguyen, and P. Marvig, *Oxidation of Metals* **90**, 2018 (1–25).
10. H. E. McCoy, *Corrosion* **21**, 1965 (84–94).
11. W. Bochnowski, Ł. Szyller, and M. Osetek, *Engineering Failure Analysis* **103**, 2019 (173–183).
12. C. Issartel, H. Buscail, and S. Mathieu, *Materials and Corrosion* **70**, 2019 (1410–1415).
13. T. D. Nguyen, J. Zhang, and D. J. Young, *Corrosion Science* **133**, 2018 (432–442).
14. T. D. Nguyen, J. Zhang, and D. J. Young, *Oxidation of Metals* **81**, 2014 (549–574).
15. T. D. Nguyen, J. Q. Zhang, and D. J. Young, *Materials at High Temperatures* **32**, 2015 (16–21).
16. T. D. Nguyen, J. Zhang, and D. J. Young, *Oxidation of Metals* **83**, 2015 (575–594).
17. H. Buscail, C. Issartel, F. Riffard, R. Rolland, S. Perrier, A. Fleurentin, and C. Josse, *Applied Surface Science* **258**, 2011 (678–686).
18. H. Buscail, C. Issartel, C. T. Nguyen, S. Perrier, and A. Fleurentin, *Matériaux & Techniques* **98**, 2010 (209–218).
19. C. Issartel, H. Buscail, C. T. Nguyen, and A. Fleurentin, *Materials and Corrosion* **61**, 2010 (929–938).
20. T. D. Nguyen, Y. Xie, S. Ding, J. Zhang, and D. J. Young, *Oxidation of Metals* **87**, 2017 (605–616).
21. J. W. Newkirk and J. A. Sago, *MRS Proceedings* **194**, 1990 (183).
22. H. Buscail, C. Issartel, F. Riffard, R. Rolland, S. Perrier, and A. Fleurentin, *Corrosion Science* **65**, 2012 (535–541).
23. H. E. Evans, D. A. Hilton, R. A. Holm, and S. J. Webster, *Oxidation of Metals* **14**, 1980 (235–247).
24. H. Buscail, R. Rolland, F. Riffard, C. Issartel, C. Combe, and P. F. Cardey, *Oxidation of Metals* **87**, 2017 (837–849).
25. S. J. Oana, *Earth Science Nagoya University* **5**, 1957 (103–124).
26. A. S. Dorcheh, M. Schütze, and M. C. Galetz, *Corrosion Science* **130**, 2018 (261–269).
27. A. Soleimani-Dorcheh and M. C. Galetz, *Oxidation of Metals* **84**, 2015 (73–90).
28. C. Wagner, *Journal of Electrochemical Society* **103**, 1956 (627).
29. A. S. Dorcheh and M. C. Galetz, *JOM* **68**, 2016 (2793–2802).
30. B. Pieraggi, *Oxidation of Metals* **27**, 1987 (177–185).
31. G. A. Greene and C. C. Finfrock, *Oxidation of Metals* **55**, 2001 (505–521).
32. D. L. Douglass, P. Nanni, C. De Asmundis, and C. Bottino, *Oxidation of Metals* **28**, 1987 (309–328).
33. B. Li and B. Gleeson, *Oxidation of Metals* **65**, 2006 (101–122).
34. W. C. Hagel and A. U. Seybolt, *Journal of Electrochemical Society*. **108**, 1961 (1146).
35. C. A. Stearns, F. J. Kohl, and G. C. Fryburg, *Journal of Electrochemical Society* **121**, 1974 (945).
36. R. J. Hussey and M. J. Graham, *Oxidation of Metals* **45**, 1996 (349–374).
37. F. H. Stott, G. C. Wood, and J. Stringer, *Oxidation of Metals* **44**, 1995 (113–145).
38. G. R. Johnston, *High Temperatures High Pressures* **14**, 1982 (695–707).
39. J. C. Slater, *Journal of Chemical Physics* **41**, 1964 (3199–3204).
40. T. Onishi, S. Nakakubo, and M. Takeda, *Materials Transactions* **51**, 2010 (482–487).
41. Solimani, A., Nguyen, T., Zhang, J., Young, D., Schütze, M. & Galetz, M. C. *Corros. Sci.* **176**, 109023 (2020).

Publisher's Note Springer Nature remains neutral with regard to jurisdictional claims in published maps and institutional affiliations.